Available online at www.sciencedirect.com
ScienceDirect
Journal of the European Ceramic Society 29 (2009) 1299–1307
www.elsevier.com/locate/jeurceramsoc

Multiple scratch tests and surface-related fatigue properties of monolithic ceramics and soda lime glass

F. Petit *, C. Ott, F. Cambier

Belgian Ceramic Research Centre, B-7000 Mons, Belgium

Received 9 July 2008; received in revised form 15 September 2008; accepted 18 September 2008
Available online 12 November 2008

Abstract

In this study, the scratch resistance of several monolithic structural ceramics and soda lime glass was investigated using repeated scratching. Rockwell indentation was used to perform unidirectional multi-pass scratches at progressive loads. It is shown that there is a build up of sample damage as the number of scratches increases, the severity of which being assessed by measuring the depth of the scratches and by performing optical observations of the worn tracks. For each applied load, there is a critical number of passes above which the material removal rate increases dramatically through chipping. By plotting the critical number of passes against the applied load, strength/number of cycles (S/N) like diagrams can be obtained. Although soda lime glass exhibits a lower resistance than most of ceramics for single scratch tests, the glass removal rate becomes similar to that of ceramics when repeated scratch tests are considered. It is suggested that the material resistance to multiple scratch tests rely on the presence of a thin layer of re-compacted and plastically deformed material under the action of the indenter. The absence of such a layer in silicon carbide may explain the surprisingly poor resistance of this material for high applied forces and important number of cycles. It is suggested that this layer improves the material resistance against scratching by decreasing the friction coefficient, thereby diminishing the level of stresses generated within the specimen.

Keywords: Wear resistance; Fatigue; Fracture; Surfaces; Scratch test

1. Introduction

Abrasive wear relates to the damage produced by sliding contact of hard particles or asperities onto a brittle surface. The material properties and the pressure at the contact area dictate the form of damages. At limited contact pressures, the material is deformed in a plastic way and a residual groove is left on its surface. At higher loads, cracking becomes the predominant mechanism and material removal may occur by chipping. As sliding contact can ultimately produce material rupture (and because it is the major cause of wear in service), it is a matter of primary importance to quantify the material resistance against sliding indentation. Unfortunately, the problem is often complicated by the fact that abrasion proceeds through successive sliding contacts and does not arise from a single scratch event. To obtain relevant information, it is therefore necessary to combine the sliding resistance of the material with its mechanical fatigue behaviour.

For many years, scratch testing has been shown to be a powerful technique to estimate the materials resistance to scratching caused by single-pass[1–3] or repeated scratch tests.[4–7] In both cases, the indenter tip is considered as a model of contacting asperity.[8,9] Since experimental conditions of scratch testing can be chosen in a wide range of parameters (sliding speed, applied force, constant or progressive load, single of repeated scratch...), the technique offers the opportunity to study the material resistance in conditions mimicking low or severe abrasion. In recent works, it was shown that repeated scratch tests can be used to study the fatigue like behaviour of coatings on substrate.[10] The authors have demonstrated that such testing process generates coating failure for a large enough number of cycles N_c. This number that depends on the contact pressure (through the applied load) and the friction coefficient between the indenter and the specimen is an intrinsic characteristic of the

* Corresponding author. Tel.: +32 65 40 34 64; fax: +32 65 40 34 60.
E-mail address: f.petit@bcrc.be (F. Petit).

0955-2219/$ – see front matter © 2008 Elsevier Ltd. All rights reserved.
doi:10.1016/j.jeurceramsoc.2008.09.019

Table 1
Experimental conditions for repeated scratch tests at progressive load.

Material	Experimental conditions: number of cycles/{applied load}
Alumina	60/{0, 30 N}
Silicon carbide	60/{0, 30 N}
Zirconia	500/{0, 30 N}
Soda lime glass	60/{0, 25 N}

coating/substrate couple. To determine N_c, a two-step procedure is usually applied. First, a scratch is performed at progressive load in order to determine the critical load for cracking. Second, unidirectional or reciprocating multi-pass scratches are performed at a load below the critical value found in the first step. The number N_c is then given by the number of cycles required to generate failure as in the single scratch test case.

The present paper extends further this approach by applying the procedure to various monolithic structural ceramics and a soda lime glass.

2. Experimental

2.1. Materials and conventional characterizations

Several brittle materials have been used in this work including some hard ceramics and a soft soda lime glass. Ceramic materials are an ultra pure alumina (99.9% post-hipped Metoxit – Switzerland), an Yttria stabilized zirconia (Metoxit – Switzerland) and a silicon carbide (ESK). The soda lime glass originates from tin float processed glass windows (AGC glass–B).

Small plates of typical size 20 mm × 20 mm × 4 mm were diamond cut from larger blocks. After cutting, the ceramic specimens were machined to become ground flat and polished with diamond pastes down to a 1 μm finish. The original faces of glass specimen were not machined in order to prevent any modification of the density and size of surface flaws. The tin face was identified using a UV lamp, all the scratch tests were carried out on the air face.

Young's modulus was determined through Impulse Excitation Technique (IET) measurements on a RFDA-HT1750 machine (IMCE – Belgium). Small rectangular bars of size 3 mm × 4 mm × 45 mm were prepared to this end. At least, five different measurements were done per specimen in order to get reliable results. Toughness was determined right after Young's modulus measurements using the SEVNB (Single Edge V-Notched Beam) method. A small sharp V-notch was saw cut within the specimen and sharpened using diamond paste and a reciprocated razor blade. The resistance of the sample was then determined using a three-point bending test apparatus using a universal testing machine (Zwick Z100 – crosshead speed of 0.1 mm/min).

2.2. Scratch testing instruments

Two scratch testers have been used in this study. A Revetest from CSEM instruments equipped with a Rockwell C diamond indenter (tip radius curvature = 0.2 mm) was used to perform single scratch test. The load was progressively raised up to 100 N over a distance of 15 mm. As usually, the critical load for chipping was determined through acoustic emission (AE) measurements and optical observations of the scratch.

To perform repeated scratch tests, a micro-combi tester (μCT) from CSM instruments was used. A Rockwell C diamond indenter (tip radius curvature = 0.2 mm) was mounted on the machine which also comprises a video microscope to perform post-scratching observations and damage diagnosis. Any scratch test was realised according to a three steps procedure. First, a "pre-scan" was performed at a very low load (0.1 N) to determine the sample profile. The "true" scratch test was realised in the second step. Finally, a "post-scan" was performed (still at load 0.1 N) to determine the depth of the residual groove after the elastic recovery. For each scratch test, several results are displayed including the applied normal load, the indenter displacement, the tangential force, the friction coefficient, the acoustic emission, the residual penetration depth and the specimen profile.

2.3. Repeated scratch test operation

The material resistance to repeated scratch tests was assessed by performing repeated unidirectional scratches at a progressive load. The load starts at 0.1 N at the beginning of the scratch and increases up to a pre-defined maximum load after a displacement of 15 mm. The final load was chosen below the critical load as determined by the single scratch test experiments. For the

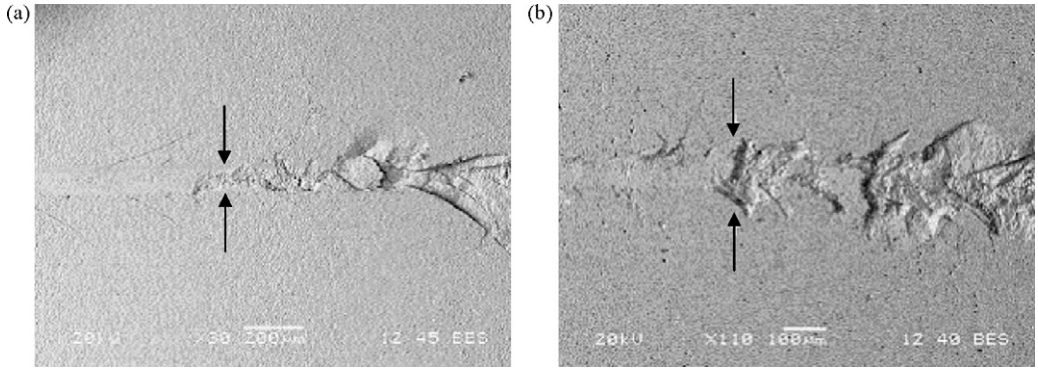

Fig. 1. Single scratch test on (a) alumina and (b) silicon carbide—the black arrows indicate the transition between cracking and chipping.

Table 2
Critical chipping load determined by single-pass scratch test.

Material	Critical chipping load (N)
Alumina	182
Silicon carbide	101
Zirconia	>200
Soda lime glass	23

conduction of these tests, 30 N was chosen for alumina, silicon carbide and zirconia while a slightly lower value (e.g. 25 N) was selected for glass. For the cyclic tests, the number of passes was experimentally adapted to exceed the threshold required for chipping. Table 1 summarizes the necessary number of cycles.

3. Results and discussion

3.1. Single-pass scratch tests

The critical load for chipping was easily determined from the acoustic emission signals. When the lateral cracks pop out at the surface of the material, a sharp increase of the acoustic emission intensity is recorded. Optical observations after scratching show that the first chips are produced simultaneously with the AE rising up. Some examples are shown in Fig. 1 for alumina and silicon carbide.

Table 2 reports the values of the critical loads for the single-pass scratch tests after averaging individual results of three different scratches. It is worth noting that these values rank in the same order than the materials toughness measured by SEVNB (same table). As there was no chipping in zirconia at 200 N, it was impossible to determine the critical chipping load for this material. Anyway, the strong damage observed by SEM and the heavily deformed scratches at 200 N suggest that the critical load does not exceed much this value, therefore, throughout this paper, we will consider that 200 N is a consistent estimation of the critical load for zirconia.

3.2. Repeated scratch tests at progressive loads

Unlike the single-pass scratch tests, acoustic emission signals are useless to determine the critical forces for chipping or cracking in cyclic loading conditions. The great amount of signals arising from indenter motions in damaged grooves, prohibits any meaningful assessment of the critical load. The only exception concerns glass for which the acoustic emission curves comprise typically three different stages (hereafter referenced as I, II and III in Fig. 2).

In the first stage (I), the AE intensity is close to zero. Optical observations of the scratch reveal the presence of a residual plastic groove only (plastic ploughing, cf. Fig. 3a). Next, the AE rises abruptly at a load which corresponds to the beginning of the second stage (part II, Fig. 2.). Observations show that the first cracks appear at this moment (Fig. 3b). They take the form of partial (due to the indenter motion) or complete Hertzian cracks which can be easily recognized through their typical circular shape. The third stage of damage (III) corresponds to a combination of both spalling and chipping. Some loose debris can be seen inside the scratch groove and on its lateral sides (Fig. 3c and d). Also, the acoustic emission signal shows a distinctive oscillatory like behaviour in this stage (part III, Fig. 2). When chipping occurs, the residual scratch depth is similarly affected by a typical oscillatory behaviour. These oscillations can be explained by the progressive building up of the damage inside the scratch groove as the load increases. Practically, the material fails along the scratch at some weakest points. When local rupture occurs, there is an increase of the material compliance and then, the indenter penetrates deeper within the sample. Acoustic emission peaks and oscillations of the penetration depth can be explained by such resulting increases of penetration depth. It must be stressed that the material removal during the third stage remains limited for low number of cycles. Most of the debris are still partially bonded to the underlying material and stay within the groove. The mean residual depth increases significantly only for large number of cycles through the removal of the debris generated during the first few passes.

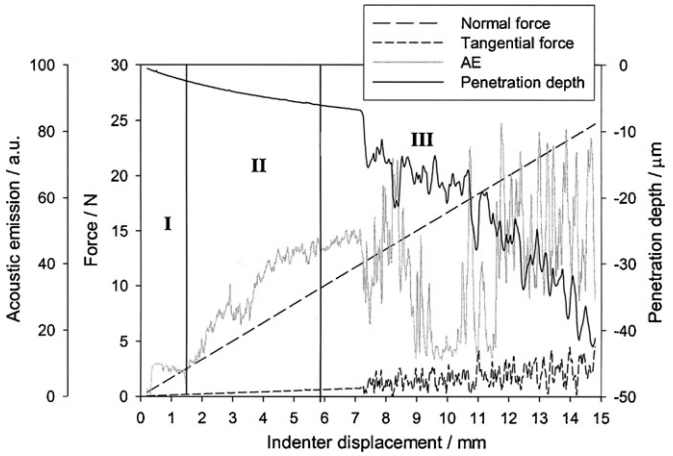

Fig. 2. Typical scratch test in glass (25 N – 10 cycles)—note the existence of three distinct behaviours (I, II and III).

By considering the change of damaging mode between two consecutives stages, the determination of the critical loads for cracking (transition between the first and second stage) and chipping (transition between the second and third stage) is possible. These evolutions are reported for the soda lime glass in Fig. 4 as a function of the number of scratches.

As expected, the number of passes required to produce significant material damaging increases as the indentation load decreases. The curves in Fig. 4 are typical for strength/number of cycles diagrams, commonly found in fatigue studies. During the first few passes, the critical force drops dramatically as a consequence of the rapid degradation of the mechanical properties of glass. After a significant number of repeats (>6 for cracking and >8 for chipping), the curves flatten out and the critical forces seem to reach two distinct asymptotic values. This result suggests that there might be a threshold indentation load below which neither cracking nor chipping occurs no matter how long the indenter is drawn onto the material surface. The asymptotic load for chipping can be seen as the endurance limit of soda lime

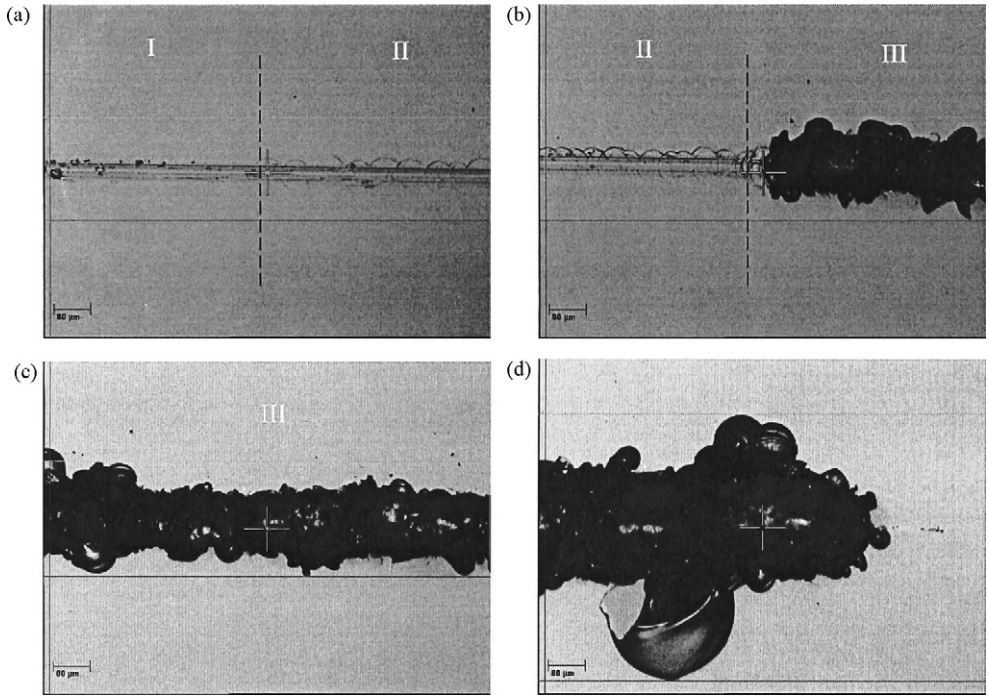

Fig. 3. Evolution of damage in glass for repeated scratch tests performed at progressive loads; (a) first transition: appearance of the first cracks; (b) second transition: formation of chips; (c) material chipping at moderate loads; (d) end of scratch: formation of large chips.

glass for the chosen set of experimental conditions: indenter tip radius, scratch velocity. . .

For ceramics, the interpretation of the results cannot be done as straightforwardly as for glass due to several complications arising from microstructural effects. As said previously, the critical cracking load for glass was determined using the AE signal combined with the optical observations of the scratches. For ceramics however, the detection of the first cracks by optical means remains a tough task. Specimen machining and polishing induces significant matrix grains pullouts which degrade the surface and make the observation of small cracks (created during scratching) a major challenge. Therefore, it was almost impossible to determine the first occurrence of cracking in alumina and only chipping was undoubtedly identified in this material. Despite the coarser microstructure of silicon carbide, the transition between the plastic deformation (at low loads) and the appearance of the first Hertzian cracks was still possible through optical means. However, such a measurement still suffers from a significant uncertainty and the variability of the results obtained that way was troublesome. To tackle all these difficulties, it was therefore necessary to consider another criterion to assess the ceramic resistance to multiple scratch tests.

Usually, the evolution of scratch width is considered to characterize the material resistance against repeated scratches. In our case however, the presence of multiple lateral damages (elongated cracks, small chips) makes this procedure not relevant. The grooves sidewalls are generally too wavy to expect obtaining reliable results, especially for shallow scratches for which surface features are sometimes undistinguishable from the scratch itself. Therefore, this procedure was not retained. It was found that the damage severity could be more efficiently described by considering the evolution of the residual depth.

Quantitative damage assessments have been undertaken by correlating the penetration depth to the applied force and the number of scratches. Our results show clearly the existence of two distinct stages for each material. For low loads and few repeated scratches, there is almost no residual penetration depth. The material deforms in a purely elastic way and a complete recovery results just after the indenter retraction. The appearance of some cracks is of course possible during this stage, but, obviously, their incidence on the penetration depth is completely obscured by the measurement accuracy. By contrast, if the load increases over a threshold value, the residual penetration depth increases suddenly as shown in Fig. 5. SEM observations

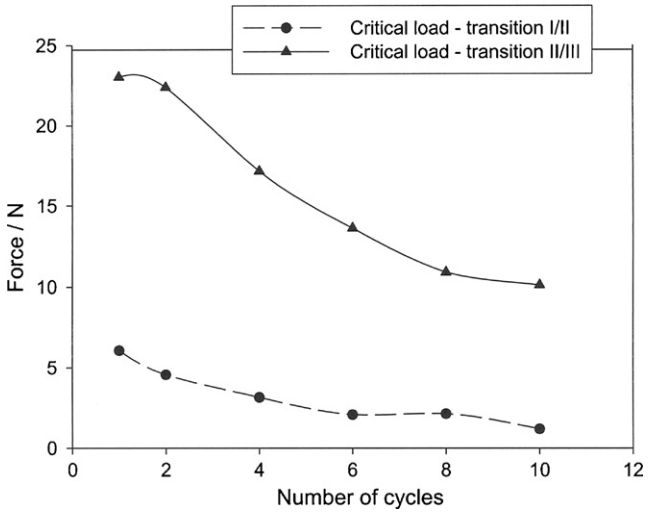

Fig. 4. Critical loads for cracking (transition I/II) and chipping (transition II/III) as a function of the number of cycles (in glass).

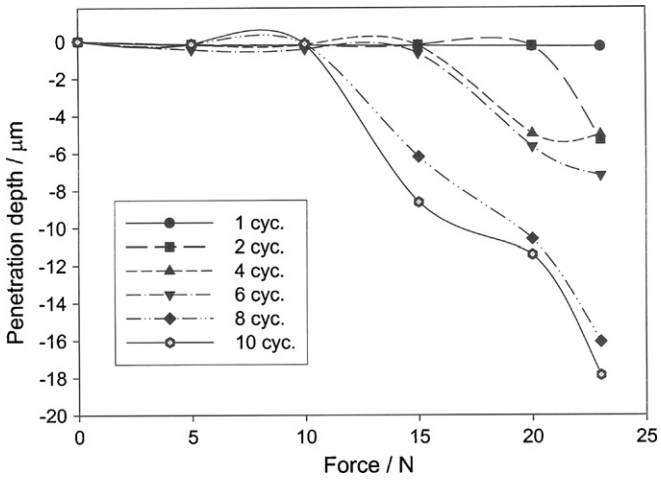

Fig. 5. Evolution of the residual penetration depth in soda lime glass for various numbers of cycles and forces.

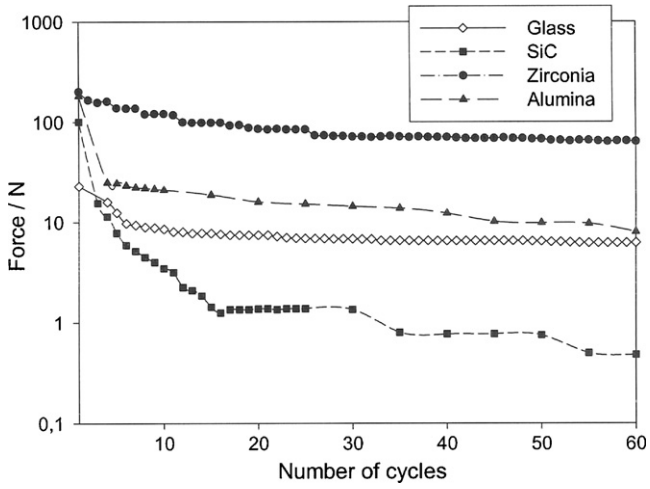

Fig. 7. Critical loads as a function of the number of cycles.

revealed that the transition between the two stages is concomitant with the formation of the first chips. Matter is removed from within the scratch and the debris formed are pushed away from the groove to accumulate along its lateral sides. It can be noted that after the transition, the penetration depth increases almost linearly with the number of passes (Fig. 6). Thanks to these observations, the position of the inflection point in the penetration depth curve can be seen as a good signal of the transition from the deformation-controlled process to the fracture-controlled process.

To measure accurately this critical load, a graphical procedure has been used. The position of the inflexion point was determined by considering the intercept of two linear fits corresponding respectively to the first and last 15% parts of the curve (example Fig. 6).

This procedure was repeated for each number of cycles and the evolutions of the critical load against the number of cycles obtained for each material are reported in Fig. 7. It is worth noting that although the curve related to glass has been obtained by a graphical means, it is quite similar to that plotted in Fig. 4

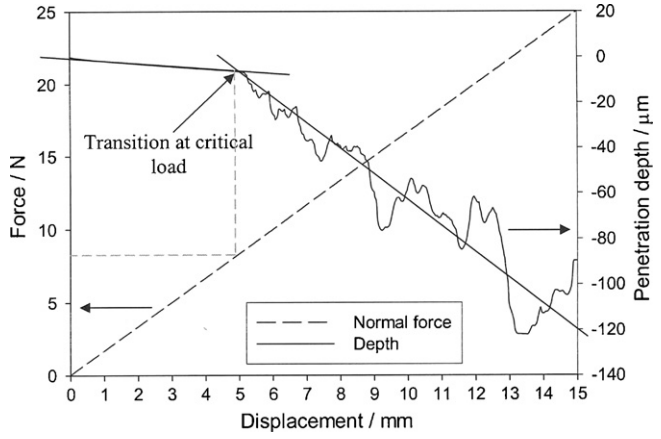

Fig. 6. Illustration of the graphical procedure used to determine the critical cracking load. For the example shown, the critical load at the intercept of the two linear fits is ≅8 N.

which was deduced from the AE signal only. The good matching of these two curves can be therefore considered as an indication of the validity of the proposed graphical procedure for the critical load determination.

As expected, all the curves exhibit a typical S–N like diagram aspect. The curves show a sharp decrease of the critical force after a few scratches, followed by a stabilization shortly afterwards.

Previously, it was also noted that the critical loads for single scratch tests rank in the same order than the materials toughness, e.g. zirconia > alumina > silicon carbide > glass. From curves shown in Fig. 7, it can be checked that such a behaviour is still observed after a few cycles. This behaviour is classically related to the fact that the critical cracking load for a Hertzian like configuration (which is similar to that involving a Rockwell indenter) varies like K_{Ic}^3/E^2. This ratio was calculated for the different materials under study and the results were noted to conform to the experimental observations (Table 3).

However, the comparison of the material resistance (as determined by the critical load) at large numbers of cycles was unexpected, especially for SiC. It can be noted that the SiC critical load is decreasing very rapidly with the number of repeats while the curves obtained for the other materials flatten out gently after only few number of repeats. At 60 cycles, the glass critical load is larger than that of silicon carbide. Obviously, the damage building up progresses more rapidly in SiC than in any of the other materials considered here. This observation is in contradiction with the traditional rule according to which the tougher and the harder the ceramic is, the better the wear resistance is.

Table 3
Estimation of the K_{Ic}^3/E^2 ratio for a single scratch test.

	SEVNB toughness (MPa m$^{1/2}$)	IET Young's modulus (GPa)	K_{Ic}^3/E^2
Alumina	3.6	380	3.2
Silicon carbide	3.1	450	1.47
Zirconia	7.1	210	81.1
Soda lime glass	0.7	70	0.7

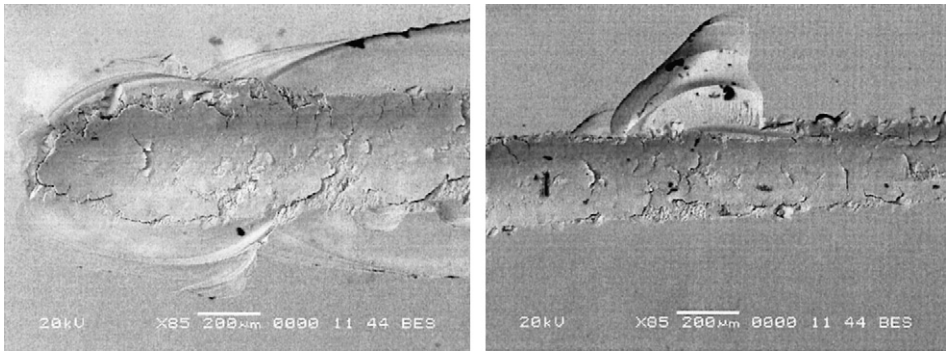

Fig. 8. Scratch grooves in glass (25 N after 30 cycles). Note the presence of a well-adhered smooth surface layer delineated by cracks.

Although the superiority of glass to silicon carbide may seem surprising, these results are in good agreement with those reported previously by Gee[11] who compared ceramics and hard metals resistance to low load multiple scratch tests. He observed that although the initial ability of some ceramics to withstand scratching damage is better than most of hard metals, the latter materials prove to be better at withstanding repeated abrasion damage by scratch test. As a possible explanation, this author suggested that an altered surface layer was formed in hard metals which might exhibit a better resistance against scratching. The good mechanical properties of this layer could arise through plastic deformation processes (work hardening) or by mechanical compaction of crushed material. In order to determine whether such explanation may apply in our case, a number of SEM observations were undertaken.

In glass, the existence of a thin layer of plastically deformed material appears as a very plausible explanation. Because sliding contact entails significant contact pressure and shear stresses, large plastic strains are expected especially in materials having low yield stress. SEM observations reveal only a few little signs of brittle damaging within the glass scratch grooves (Fig. 8). Contrarily, the tracks exhibit a typical smooth aspect which suggests that there is a well-adhered thin layer of plastically deformed glass. The worn surfaces show many flat areas delineated by networks of cracks and, in some rare places, rougher depressed areas (Fig. 8b).

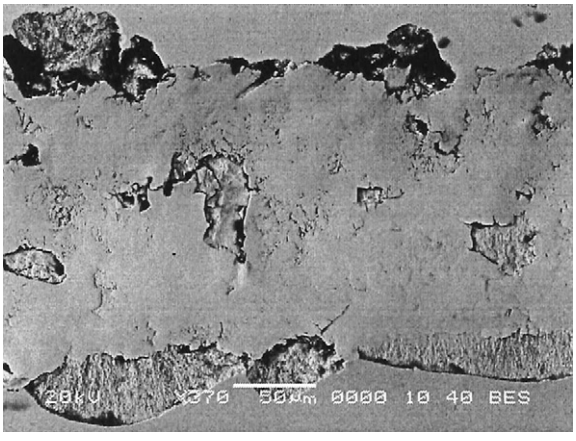

Fig. 9. Scratch groove in zirconia at 30 N (after 500 cycles)—note the presence of large flat areas of worn matter.

A very similar pattern was also noted in zirconia. As shown in Fig. 9, large flat areas can be identified and the pictures also support the existence of a thin layer of plastically deformed material.

For comparison purposes, Figs. 10 and 11 show the observations carried out in alumina and silicon carbide in similar experimental conditions (force and number of cycles). Although there is still some evidence suggesting that plastic deformation occurs in those materials, the materials exhibit now important spallation; the thin surface layer is either partly visible (alumina) or totally absent (SiC). In the latter case, the subsurface microstructure is easily detected. Similar observations made after different number of cycles suggest that no such similar layer forms in silicon carbide.

At higher magnification, the flat areas observed in the wear tracks of glass, alumina and zirconia reveal a complex structure. The observations show that they are partly obtained through the agglomeration of very small debris, obviously formed during the first passes of the indenter. Moreover, there is clear evidence that this crushed matter has been subsequently compacted and heated under the repeated action of the indenter. The vitreous like aspect of the crushed matter (Fig. 12) is typical from a local melting (or sintering). All these observations suggest that the observed flat areas result probably from the combination of crushed material compaction and plastic deformation at high temperatures and pressures, as suggested previously by Gee for hard metals.

It is interesting to compare those results with those obtained for SiC. For large number of cycles, SEM observations of SiC grooves reveal that the material becomes increasingly fragmented and there are strong evidences that damage occurs mainly through intergranular fracture (Fig. 13).

It is reasonable to assume that the important decrease of the SiC resistance arises from a significant material fragmentation, not followed by re-compaction and plastification. The influence of microstructure and grain size has to be considered as a first possible explanation of this specific behaviour. In ref. [12] it was underscored that the matrix grain size exerts a considerable influence on the damaging mode during repeated scratching. Although the results were established for alumina, we can reasonably extrapolate them to the case of SiC also. In this reference, it was sketched that for fine-grained alumina, subsurface damage consists mainly of intra-grain twin/slips bands within the plastically deformed zone. On the contrary, the nature

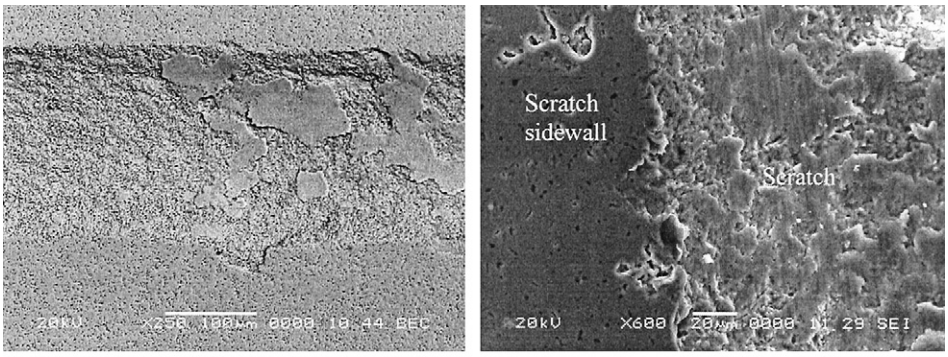

(a) alumina (b) silicon carbide

Fig. 10. Scratch grooves observed on ceramics. (a) Some remnants of the plastically deformed layer are still visible on alumina. (b) On silicon carbide, no plastic layer is observed and only very small areas of smooth surface are noticed.

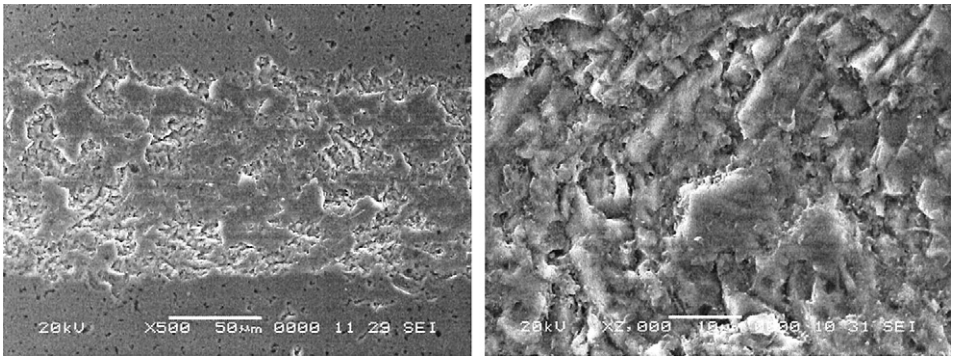

Fig. 11. Some views of a groove in silicon carbide showing important intergranular fracture.

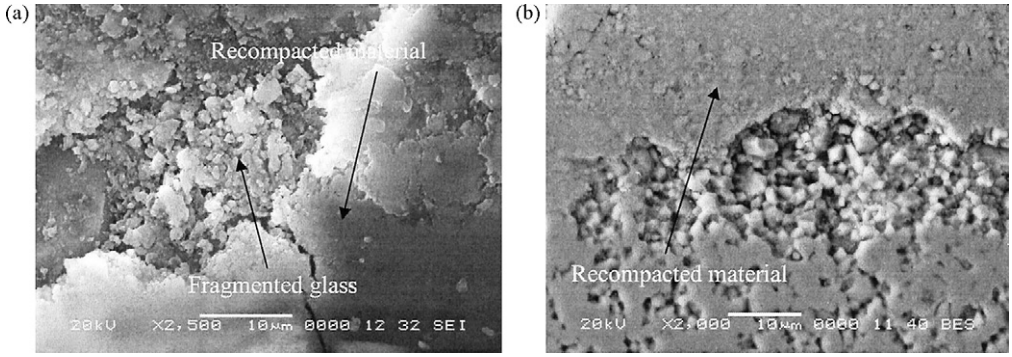

Fig. 12. Higher magnifications of the scratch grooves in (a) glass and (b) alumina showing the presence of re-compacted crushed material.

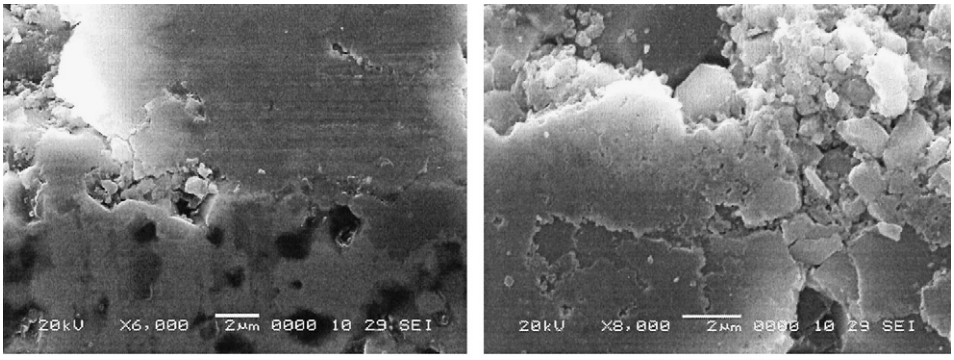

(a) alumina (b) silicon carbide

Fig. 13. Views of the inside of the grooves in alumina and silicon carbide after 20 cycles.

of subsurface damage in coarse-grained alumina was reported to be of a different nature and more severe. For such material, damage consists primarily of intergranular microcracks and grains dislodgments. When considering the SiC curve in Fig. 7, it can be noted that critical loads never reaches a plateau as in the other S/N curve. In fact, it decreases continuously to reach values well below 1 N. If the mechanism of SiC damaging is similar to that reported in literature for coarse-grained alumina, then it could explain the observed continuous damage building up with the number of cycles. On the contrary, our fine-grained alumina and zirconia are clearly less sensitive to grain dislodgment and material removal.

The rapid degradation of SiC prohibits any rigorous assessment of the fatigue limit of this material. For the other materials, the existence of an endurance limit appears more relevant. For zirconia, alumina and glass, the fatigue limit, determined by the asymptotic value of the curves shown in Fig. 7 is estimated to be 64 N, 9.8 N and 6.2 N, respectively. A tentative evaluation for silicon carbide gives a value below 0.5 N. Except for this material, the resistance of the other grades rank in the conventional order given by the K_{Ic}^3/E^2 ratio.

It may be noted that the hardest the material is or the coarsest the microstructure is, the fastest the material degrades with the number of passes (alumina and silicon carbide). Traditionally, a high hardness and a coarse grain size (which governs the grain boundaries strength) are considered as unfavourable characteristics for obtaining a satisfying smooth polishing state. Therefore, one may wonder whether the fast degradation of silicon carbide does not arise from the presence of residual asperities at the surface, not fully eliminated during the polishing stage. When those asperities come into contact with the indenter, very high pressures are generated since the true contact area differs then from the load bearing one. Those high pressures should certainly be large enough to form cracks just below the material surface. Then, when the indenter is driven back again at the same place, the material breaks up more easily and the penetration depth increases subsequently. Moreover, during repeated scratching, the debris formed by grains dislodgment are entrapped within the scratch groove. This matter exerts certainly an additional contribution to wear through third body abrasion. Although this explanation is probably not consistent for glass, zirconia or alumina where smooth scratch grooves have been observed, it could be relevant for explaining the results in SiC where considerable fracture occurs.

In order to better understand the singular behaviour of SiC, it is also useful to consider the evolution of the friction coefficient with the number of cycles. These results are reported in Fig. 14 and compared with measurements performed on the other materials. Since our goal was a qualitative assessment of the friction coefficients, this graph was simply obtained by considering the averaged value of the friction coefficient taken along the whole scratch length (regardless of the applied force and/or damage occurrence).

Silicon carbide exhibits a much higher coefficient of friction. It can be as high as 0.55 after 20 cycles to decrease slowly afterwards. Such huge value can be related either to the larger surface roughness developed by wear, to a slip-stick mechanism and/or more probably to the injection of wear debris at the indenter/material interface as suggested above. Anyway, it is well known that the effect of sliding with friction is to add a compressive stress to the front edge and to increase the tensile stress at the trailing edge. A simple Hertz contact analysis then shows that the magnitude of the developed tensile stress is directly related to the applied normal force and the coefficient of friction. Therefore, as the coefficient of friction increases, a lower force is needed to initiate fracture by microcracking. As a consequence of the large friction coefficient in SiC, crack nucleation occurs probably more easily in this material.

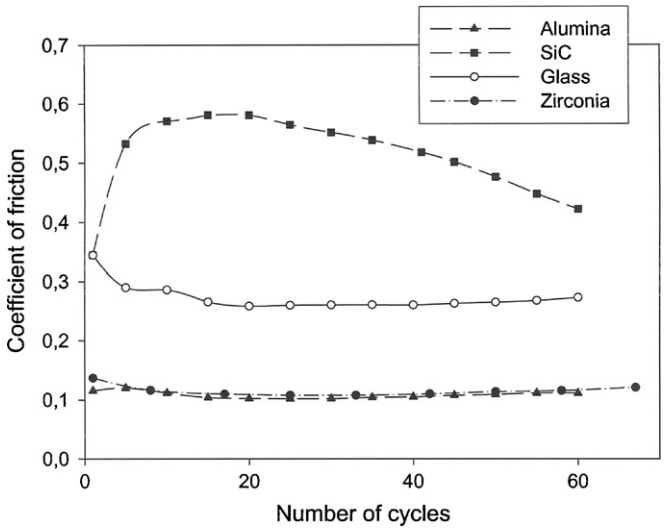

Fig. 14. Evolution of the coefficients of friction with the number of repeats.

The reason why there is no re-compacted/plastically deformed layer in SiC is not really fully clarified. It could be related to the presence of a thin layer of brittle SiO_2 at surface and/or to the high hardness and thermal properties of SiC. The huge hardness of SiC ($H_v > 2500$) limits the material ability to plastification even at high contact pressures. Moreover, the high thermal conductivity of SiC favours the rapid cooling of the surface when repeated scratch tests are performed. Therefore, the conditions of local melting or sintering of the crushed material can hardly be reached on the contrary to the other studied materials. The problem of the thermal exchange between sliding bodies was discussed in literature a long time ago. For friction contact between two bodies, elevation of temperature is related to the Peclet number *Pe* given by:

$$Pe = \frac{Vl}{2\chi} \tag{1}$$

where V is the displacement velocity of the moving thermal source (the indenter in our case), l is one half of the thermal source length and χ is the thermal diffusivity. The temperature increase can be assessed by considering the mean temperature elevation θ_m and the local temperature elevation at the interface, the so-called "flash temperature" θ_M. Derivation of analytical expressions of both θ_m and θ_M are possible and each value is related to *Pe*. For a large Peclet number (corresponding to a fast displacement velocity), the generated heat at the interface cannot diffuse easily through the material thickness. The heat

flux stays confined close to the surface on a very thin layer and the temperature of this small volume of matter increases considerably. For a circular contact between the two bodies and large Peclet number, θ_m and θ_M are given by[13]:

$$\theta_m = \frac{\pi}{3.251}\frac{q}{\lambda}\left(\frac{\chi l}{V}\right)^{1/2} \quad \text{and}$$

$$\theta_M = 0.726\gamma\mu\sigma_y\left[\frac{V}{\lambda\rho C}\sqrt{\frac{F_N}{\sigma_y}}\right]^{1/2} \tag{2}$$

where q is the density of the thermal flux, λ and ρ are the thermal conductivity and the density of the substrate, respectively and F_N and σ_y are the normal load and the material yield stress, respectively. γ is related to the Peclet number but changes only slightly. Typical values range between $\gamma = 0.72$ for $Pe = 5$ and $\gamma = 0.92$ for $Pe = 100$.

If one considers that "crushed material re-compaction" occurs at high temperatures, then we are mainly interested in θ_M. It is worth noting that θ_M increases with the friction coefficient and with the material yield stress (which can be considered as roughly proportional to the hardness H_v). Moreover, it is inversely proportional to the material density and thermal conductivity. Therefore, the "ability" of material re-compaction with formation of news bonds between crushed pieces can be estimated by the parameter:

$$\eta = \frac{(\mu H_v^{3/4})}{(\lambda\rho)} \tag{3}$$

Calculation of η gives 0.36, 1.77, 0.08 and 13.32 for alumina, zirconia, silicon carbide and glass, respectively. It is remarkable that despite all roughness of this calculation, the obtained η values are perfectly consistent with our experimental results. According to the η values, the material ability for the formation of bonds (or which is the same, for the formation of a thin surface layer with specific mechanical properties) between crushed pieces, rank in the order glass > zirconia > alumina > silicon carbide. Therefore, it is confirmed that silicon carbide is particularly deficient in conditions of severe scratching.

4. Conclusions

In this paper, the resistance of several ceramics and glass to multiple scratch tests was studied. A graphical method to determine the critical load from the deformation-controlled to fracture-controlled process was proposed. It was shown that the curve of the critical load against the number of passes exhibits a typical S/N aspect, thereby demonstrating that a fatigue like mechanism is involved in the damaging. Distinct material behaviours were observed. In zirconia, glass and, in some extent, in alumina, the presence of a thin layer of re-compacted crushed material was suggested to be beneficial to the material resistance by limiting the friction. By contrast, the damaging of SiC was noted to mainly result from intergranular cracking in conjunction with a dramatic increase of friction. Since obtaining a complete S–N curve using conventional techniques is a tedious and expensive procedure, the multiple scratch test method can be seen, in some cases, as a very attractive alternative.

Acknowledgement

The financial support of the Belgian SPF Economy is gratefully acknowledged (contract number CC CCN–105).

References

1. Perry, A. J., Scratch adhesion testing of hard coatings. *Thin Solid Films*, 1983, **107**, 167.
2. Steinmann, P. A. and Hintermann, H. E., Adhesion of TiC and Ti(C, N) coatings on steel. *J. Vac. Sci. Technol.*, 1985, **43**, 2394.
3. Valli, J., A review of adhesion test methods for thin hard coatings. *J. Vac. Sci. Technol., A*, 1986, **4**, 3007.
4. Bull, J. and Rickery, D. S., Multi-Pass Scratch Testing as a model for abrasive wear. *Thin Solid Films*, 1989, **181**, 545.
5. Von Stebut, J., Scratch testing induced surface damage of thin coatings; a study of failure mechanisms by means of appropriate surface analytical tools. In *Plasma Surface Engineering (PSE 1988)*, ed. E. Broszeit, W. D. Münz, H. Oechsner, K.-T. Rie and G. K. Wolf. DGM, 1989, p. 1215.
6. Darbeida, A., Von Stebut, J., Assoul, M. and Mignot, J., A Multi-pass/scanning tribometer for on-line friction and wear mapping. *J. Mech. Tools Manufact.*, 1995, **35**, 177.
7. Efeoglu, I. and Arnell, R. D., Multi-pass sub-critical load testing of titanium nitride coatings. *Thin Solid Films*, 2000, **377–378**, 346.
8. Swain, M. V., Microfracture about scratches in brittle solids. *Proc. R. Soc.*, 1979, **A336**, 575.
9. Zhang Bi, Tokura, H. and Yoshikawa, M., Study on surface cracking of alumina scratched by single-point diamonds. *J. Mater. Sci.*, 1988, **23**, 3214.
10. Von Stebut, J., Multi-mode scratch testing–a European standards, measurements and testing study. *Surf. Coat. Technol.*, 2005, **346–350**, 200.
11. Gee, M. G., Low load multiple scratch tests of ceramics and hard metals. *Wear*, 2001, **250**, 264.
12. Hockin, H., Xu, K. and Jahanmir, S., Microfracture and material removal in scratching of alumina. *J. Mater. Sci.*, 1995, **30**, 2235.
13. Archard, J. F., The temperature of rubbing surfaces. *Wear*, 1958, **2**, 438–455.